

Energy Transfer Pathways in the CP24 and CP26 Antenna Complexes of Higher Plant Photosystem II: A Comparative Study

Alessandro Marin,[†] Francesca Passarini,[‡] Roberta Croce,[‡] and Rienk van Grondelle^{†*}

[†]Faculty of Sciences, Vrije Universiteit Amsterdam, Amsterdam, The Netherlands; and [‡]Department of Biophysical Chemistry, Groningen Biomolecular Sciences and Biotechnology Institute, University of Groningen, Groningen, The Netherlands

ABSTRACT Antenna complexes are key components of plant photosynthesis, the process that converts sunlight, CO₂, and water into oxygen and sugars. We report the first (to our knowledge) femtosecond transient absorption study on the light-harvesting pigment-protein complexes CP26 (Lhcb5) and CP24 (Lhcb6) of Photosystem II. The complexes are excited at three different wavelengths in the chlorophyll (Chl) Qy region. Both complexes show a single subpicosecond Chl *b* to Chl *a* transfer process. In addition, a reduction in the population of the intermediate states (in the 660–670 nm range) as compared to light-harvesting complex II is correlated in CP26 to the absence of both Chls *a*604 and *b*605. However, Chl forms around 670 nm are still present in the Chl *a* Qy range, which undergoes relaxation with slow rates (10–15 ps). This reduction in intermediate-state amplitude CP24 shows a distinctive narrow band at 670 nm connected with Chls *b* and decaying to the low-energy Chl *a* states in 3–5 ps. This 670 nm band, which is fully populated in 0.6 ps together with the Chl *a* low-energy states, is proposed to originate from Chl 602 or 603. In this study, we monitored the energy flow within two minor complexes, and our results may help elucidate these structures in the future.

INTRODUCTION

Photosynthesis is the process whereby sunlight energy is used to convert carbon dioxide into organic compounds. In plants, sunlight is absorbed by pigments bound to the light-harvesting pigment-protein complexes (Lhc) of Photosystem (PS) I and II. Subsequently, excitation energy is transferred to the reaction center, where conversion into chemical energy takes place. The properties of the Lhcs of PSII have been intensely studied to pursue a better understanding of the energy transfer processes (1–3) and of NPQ photoprotection mechanism, in which excess excitation energy is dissipated into heat (4–8). In the PSII of higher plants, six gene products belonging to the Lhc family constitute the antenna system (9). The major antenna complex, LHCII, is a heterotrimer composed of the Lhcb1–3 gene products. Three other Lhcs, the so-called minor antennas, are present in PSII: CP29, CP26, and CP24 as encoded by the Lhcb4, Lhcb5, and Lhcb6 genes, respectively. These antennas are located between the LHCII trimers and the core complex, where primary energy conversion reactions take place (10). Thus, they are largely involved in the delivery of the excitation energy to the reaction center (11). However, clear data on the different roles played by the individual complexes in light-harvesting and photoprotection are still lacking.

The x-ray structure of LHCII allowed investigators to assign pigment identity and orientation (12,13). LHCII hosts per monomeric unit six chlorophylls (Chls) *b*, eight Chls *a*, and four carotenoids ((Cars); two luteins (Lut) in the central L1 and L2 sites, one neoxanthin (Neo) in the N1 site, and one violaxanthin (Vio) in the V1 site). No structures are

available for the minor antenna complexes, although sequence homology with LHCII suggests a very similar structural organization (14). It has been suggested that minor antenna complexes coordinate a smaller number of Chls as compared to LHCII (i.e., eight for CP29, nine for CP26, and ten for CP24) (15,16). Researchers have employed *in vitro* reconstitution (17–20) coupled with mutation analysis (21–26) to elucidate the structure/function of these complexes. The results led to a map of the occupation of pigment-binding sites, which represents the starting point for understanding the functional architecture of these complexes. The next step is to integrate structural data with time-resolved spectroscopic results, but to date this has been done only for LHCII and CP29 (1,27,28).

Previous experiments on native trimeric and monomeric LHCII, carried out at 77 K (29–32), revealed similar dynamics for the two types of complexes. Notably, it was inferred that Chl *b* excitation energy transfer (EET) occurred more slowly and to Chls *a* absorbing at higher energies in monomers than in trimers. One obvious reason for this is the destruction of the Chl *b* cluster (*b*601(1), *b*608(2), and *b*609(2)) at the interface of two monomers, and the fact that due to the absence of intermonomer energy transfer, the final state is bluer and broader. It was concluded that the intramonomeric energy transfer in native trimeric LHCII can explain many of the fast Chl *b* to Chl *a* singlet excitation transfer processes and the slow dynamics between Chls *a*. However, the relatively high pump intensities used for these experiments put the results outside the annihilation-free regime.

More recently, Novoderezhkin et al. (27) and Palacios et al. (33) studied LHCII and monomeric or homotrimeric recombinant Lhcb1–3 complexes at 77 K by exciting in

Submitted August 1, 2010, and accepted for publication October 19, 2010.

*Correspondence: r.van.grondelle@few.vu.nl

Editor: Leonid S. Brown.

© 2010 by the Biophysical Society
0006-3495/10/12/4056/10 \$2.00

doi: 10.1016/j.bpj.2010.10.034

the Chl Qy region. EET from Chl *b* to Chl *a* mainly occurred rapidly, with two sub-ps components (130 and 600 fs) followed by a slower ~3 ps phase from the Chls absorbing in the intermediate-state region (660–670 nm) between the major Chl *b* and Chl *a* Qy bands. The heterogeneous dynamics found in the Chl *b* Qy band were explained by equilibration within two Chl *b* bands. Excitation at 661 nm showed a fast process (0.5–0.6 ps) from red-shifted Chls *b* to Chls *a* followed by slower dynamics (~2.5 ps) between Chls *a*. In general, the lifetimes found for the different isoforms were similar, and a high homology between the complexes was suggested.

Several transient absorption (TA) studies were undertaken on LHCII and on the minor antenna CP29, focusing on Chl-Chl dynamics both at room temperature (34–37) and at 77 K (38,39). The room-temperature TA measurement on CP29 after 640 and 653 nm excitation showed three Chl *b* to Chl *a* EET lifetimes of 0.15, 1.2, and 5–6 ps, along with a lifetime of 0.6–0.8 ps for the Chl *b* absorbing at 640 nm (38). In a study of CP29 at 77 K, Gradinaru et al. (38,39) reported lifetimes of 0.22–0.35 and 2.2 ps for Chls *b* absorbing at 640 nm, 2.2 ps for Chls *b* absorbing at 650 nm, and a slower ~10 ps component for both Chl *b* pools. Two components of 0.28 and 10 ps describing EET from blue to red Chls *a* were also found. Notably, in a temperature-dependent study of energy transfer in LHCII, Savikhin et al. (40) observed only small differences between data obtained at 77 K and at room temperature.

In this work, we performed femtosecond pump-probe measurements to study the EET dynamics in CP24 and CP26, and obtain information for a full characterization of the light-harvesting process in the antenna complexes of PSII. In addition, the differences in EET dynamics among members of the Lhc family are discussed with the aim of understanding the role played by each antenna in light-harvesting and photoprotection.

MATERIALS AND METHODS

Sample preparation

Mature DNA sequences coding for CP24 (AT1G15820) and CP26 (AT4G10340) were amplified from an *Arabidopsis thaliana* cDNA library by polymerase chain reaction using specific primers. Amplified sequences were then cloned in a modified pET-28a(+) vector carrying a minimum polylinker and overexpressed in the Rosetta2(DE3) strain of *Escherichia coli*. Apoproteins were purified as inclusion bodies, and pigment-protein complexes were reconstituted as previously described (41) using a mix of purified pigments extracted from spinach with a Chls *alb* ratio of 2.9 and a Chls/Cars ratio of 2.7. Purification of the antenna complexes from unfolded proteins and free pigments was performed as described previously (26).

77 K steady-state absorption spectra and pigment content analysis

We recorded 77 K absorption spectra using a Cary4000 spectrophotometer (Varian, Palo Alto, CA) at a Chl concentration of ~6 μg/mL in 10 mM

TABLE 1 Pigment content of the CP26 and CP24 protein complexes

	Chl <i>a/b</i>	Chl/Car	Chl <i>a</i>	Chl <i>b</i>	Lut	Vio	Neo	Chls
CP26	1.92	3.88	5.91	3.09	1.40	0.08	0.85	9.00
CP24	1.00	5.23	5.01	4.99	0.97	0.95	0.00	10.00

Values are normalized to the proposed total number of Chls reported in the last column. The error is <5%. Lut, lutein; Vio, violaxanthin; Neo, neoxanthin.

HEPES pH 7.5, 0.03% β-DDM, and 70% v/v glycerol. The pigment complement of CP24 and CP26 complexes was extracted from the antenna complexes with 80% acetone (v/v). It was analyzed by integrating data obtained independently with two methods: high-performance liquid chromatography (42) and fitting of the acetone extracts. The fitting consisted of comparing the acetone extract spectrum with the spectra of individual pigments as described previously (43). The pigment content is reported in Table 1.

Femtosecond TA setup

Femtosecond laser pulses were obtained with a seed laser (Vitesse-2W; Coherent, Santa Clara, CA) and a regenerative amplifier (Legend USP-1K-HE; Coherent) pumped by the second harmonic of an Nd:YLF laser (Evolution-30; Coherent). The output of the amplifier was 2.5 mJ per pulse at 1 kHz, with a duration of <40 fs at 800 nm. The output was split into two beams: one beam was focused into a CaF₂ plate to generate a white-light continuum for the probe pulse, and the other was used to pump an infrared optical parametric amplifier (Opera-HE-USP-1K; Coherent). The output of the OPA was tuned to 1264, 1304, or 1324 nm and frequency-doubled in a BBO crystal to generate 632, 652, or 661 nm pump pulses. After frequency doubling was achieved, a low-pass filter was used to block the residual of the fundamental. To achieve a higher selectivity upon excitation, interference filters were used with central wavelengths of 632, 652, and 661 nm, and bandwidths of 10.6, 9.4, and 9.8 nm, respectively. The instrument response function of the system was 112 fs, estimated from the full width at half-maximum (FWHM) of the cross-correlation signal measured after mixing pump and probe beams in a BBO crystal at the position of the sample. A magic angle configuration was adopted for the mutual orientation of pump and probe polarizations by rotating the polarization of the pump with a Berek polarizer. The time difference between the pump and the probe was adjusted by changing the pump beam path length through an optical 60 cm-long delay line (M-IMS600CHA; Newport, Irvine, CA). Via a phase-locked chopper, the repetition rate of the pump was lowered to 500 Hz. In this way, pumped and unpumped absorption spectra were successively acquired shot-to-shot at 1 kHz with an in-house-built photodiode array (PDA) detector. The pump and probe beams were then focused in the sample. The diameter of the probe in the focus was ~115 μm FWHM. The overlap of the pump and probe at the focus was optimized with the pump entirely covering the probe. After collimation was completed, the probe was sent into a spectrograph and detected with an in-house-built PDA detector. The PDA (S4801; Hamamatsu, Hamamatsu City, Japan) had 256 × 2 pixels over a length of 32.0 mm, giving a spectral resolution of 1.2 nm. Excitation intensities of 1.34–3.0 nJ/pulse were used. All measurements were carried out at 77 K on samples contained in a 1 mm cuvette with absorption OD = 0.4/mm.

Data analysis

The recorded TA data were analyzed simultaneously with a global analysis fitting routine described previously (44). Time-resolved data probed at different wavelengths were fitted together using an irreversible kinetic model consisting of sequentially interconverting compartments connected

by successive monoexponential decays of increasing time constants. The model yields difference spectra, termed evolution-associated difference spectra (EADS), each of which decays with a corresponding lifetime. A Gaussian instrument response function with FWHM ~ 112 fs was necessary to fit the TA data after pump excitation. The group velocity dispersion of the probe was parametrized with a third-order polynomial. The first EADS corresponds to the state after excitation, and the next EADS, which contains mixtures of several species, portrays the evolution of the excited states of the system.

RESULTS

OD spectra

In Fig. 1, the 77 K absorption spectra of CP26 and CP24 are displayed along with their second derivative. CP26 in the Qx/Qy region shows a characteristic spectrum with three peaks at 676.4, 650.8, and 636.2 nm. CP24 peaks in the Qy region at 669.6 nm and has a shoulder at 675.5 nm. The Chl *b* band peaks at 650.0 nm and, similarly to CP26, a Chl *b* absorbing at high energies is discernible by the shoulder it forms around 637.6 nm. The Soret region reflects different Chl and Car content in the systems.

CP26, 652 nm excitation

Pump-probe experiments with excitation at 632, 652, and 661 nm were carried out on CP26 and CP24. Pump-probe traces at different excitation and detection wavelengths are shown in Fig. 2. For the global analyses of CP26, excited at 652 or 661 nm, four components were minimally required to describe the data. A fifth component was needed in the CarT region at late delay times (see Fig. 5). The first spectrum of the analysis after 652 nm excitation (Fig. 3 B) shows a bleach peaking at 651.5 nm and a flat bleach/stimulated emission (SE) band covering the Chl Qy 660–675 range. The presence of excited Chls dispersed over the whole Qy

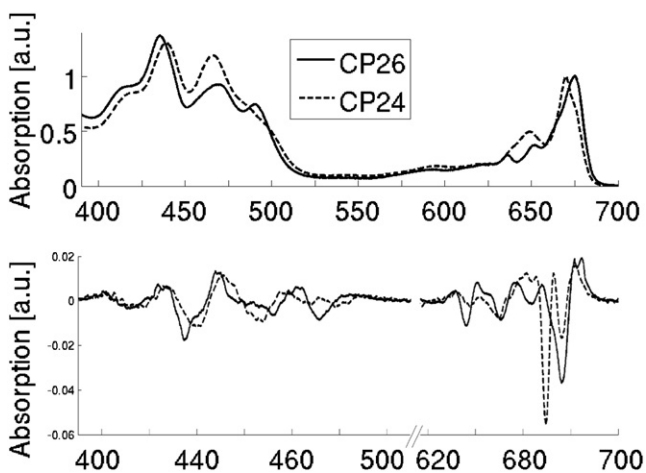


FIGURE 1 77 K absorption spectra of CP26 and CP24 (*top*), and the second derivative (*bottom*). The spectra were normalized at the maximum OD of the Qy region.

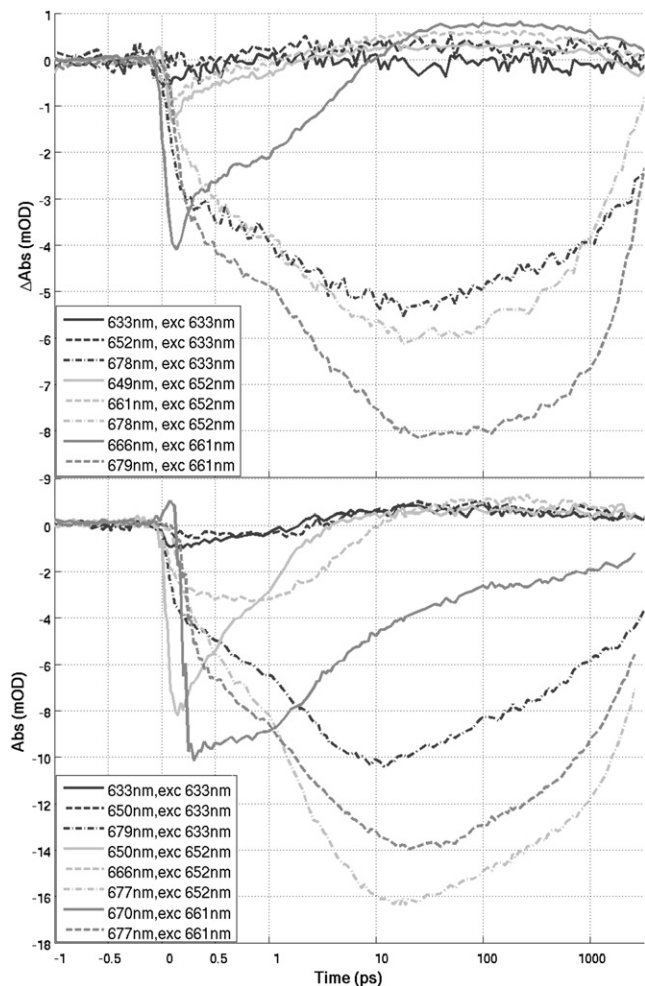


FIGURE 2 Kinetic traces for CP26 (*top*) and CP24 (*bottom*) at 77 K. The detection and excitation wavelengths are indicated in the legends.

region implies that either partial energy transfer from Chls *b* to *a* has already occurred on a timescale < 100 fs, or that Chls *a* were excited directly in the Qy vibronic band. Below 620 nm (not shown) a flat Chl *a* and *b* excited state absorption (ESA) appears, followed at wavelengths shorter than ~ 500 nm by the bleach/SE of the Chl *b* Soret band.

A lifetime of 210 fs leads to the second component of the global analysis. Clearly, excitation has moved from the Chl *b* to the Chl *a* states at 677 nm. In the second spectrum, the area of the 652 nm band has decayed by 60%, whereas the Chl bands above ~ 670 nm have increased. The second 1.5 ps component results in the complete decay of the Chl *b* excited states and a reduction of the high-energy flank to the Chl *a* Qy bleaching. The decay-associated difference spectra (DADS), i.e., the plots of the amplitudes associated to the exponential decays (44) (see Fig. S1 of the Supporting Material) give more insight into the Chl *b* decay. The fastest 210 fs transition shows the decay of a Chl *b* population at 650 nm, whereas in the subsequent 1.5 ps transition the decaying Chl *b* band is centered at 653–654 nm. This behavior

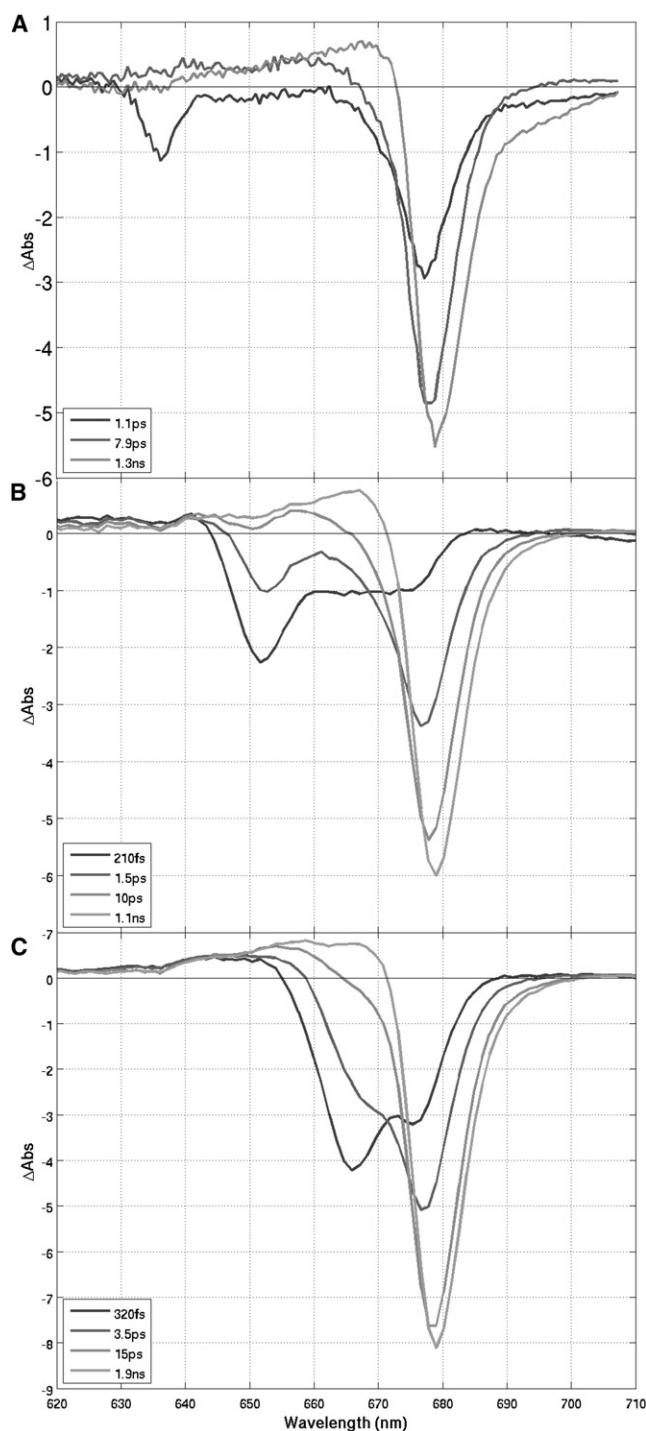


FIGURE 3 Global analysis of CP26 excited at 632 nm (A), 652 nm (B), and 661 nm (C).

is similar to what was found by Palacios et al. (33) for monomeric or homotrimeric recombinant Lhcb1–3 complexes, meaning that different Chl *b* populations are present, and the higher-energy population (650 nm) decays faster than the lower-energy population (653–654 nm). In addition, the first two transitions also show the decay in

the intermediate-state region of bands centered at 660–665 and 663–668 nm (cf. the first and second DADS in Fig. S1, respectively). A comparison of the ESA of the third and fourth EADS in Fig. 3 B indicates that a slowly decaying population of intermediate states absorbing at relatively high energies (~660–675 nm) overlaps with the Chl *a* ESA, shifting the bleach/SE peak in the third spectrum to slightly higher energies (i.e., to 678 nm). Therefore, the second evolution shows, next to the decay of Chls *b*, a faster phase of the intermediate states. However, the contribution of these intermediate states is much less evident in CP26 than in LHCII and LHCII components (33), suggesting that these states are less populated.

The last component in Fig. 3 B, which shows a peak at 679 nm and an ESA at shorter wavelengths, represents the equilibrated spectrum. The Chl *a* bleachings in our experiments decay in 1.1–2.4 ns, although a precise determination of such a lifetime is limited by the length of the delay line used (3.4 ns). The intermediate states decay in 10 ps to the reddest Chls *a*, which slightly increase in population.

An additional infinite component was needed to correctly fit the features appearing at late delay times in the ~480–520 nm range (the EADS are shown in Fig. 5). The component is associated with the rise of a Car triplet (CarT), formed after the slow Chl triplet (ChIT) formation and fast ChIT-to-CarT transfer (45). All EADS in Fig. 5 show a bleaching at 490–495 nm and a maximum ESA at 511 nm, and thus are 3–5 nm red-shifted as compared to the RT spectrum of CP26 (46). This difference is likely due to the fact that at 77 K only the triplet state of Lut-L1 is populated, since at this temperature most of the excitation ends up in the lowest Chl states (Chl *a*610–*a*612), lying close to the Car in the L1 site (Lut) (47).

CP26, 661 nm excitation

The EADS appearing at time zero (Fig. 3 C) shows a bleach/SE with minima at 666 and 675 nm. The band at longer wavelengths originates from both direct excitation and ultra-fast (<100 fs) energy transfer from the excited pigments to the Chls *a*. Compared to the EADS previously reported for LHCII and LHCII components (see Fig. 7 in Palacios et al. (33)), the first peak is red-shifted by several nanometers and the peak at 675 nm is more pronounced, suggesting that EET to low-energy Chls *a* is more efficient in CP26. Similar to the 652 nm data set, a flat Chl *a/b* ESA fills the 500–635 nm range in all EADS. Only in the first spectrum is a small bleach/SE at 472–479 nm present, implying that a fraction of Chls *b* (estimated in 10% of the total Qy bleaching) is excited at 661 nm, and that it belongs to the Chl *b* population transferring to Chl *a* in the sub-ps range. During the 3.5 ps transition, EET from intermediate states to Chls *a* took place. The EADS in fact is composed of a bleach/SE at 676.5 nm and a pronounced shoulder at ~668 nm. The first two evolutions, with lifetimes of 320 fs

and 3.5 ps, thus describe two phases of the EET from Chls *b* and blue Chls *a* to Chls *a* absorbing at lower energies. Similar to the 652 nm data set, some residual long-lived states are noticeable in the ~660–675 nm range of the third spectrum, since a shoulder is present at ~666 nm, which decays in the last evolution (15 ps). As in the case of CP26 excited at 652 nm, the fourth component is uniquely composed of equilibrated Chl *a* excited states, since the long-lived Chl *a* excited states at ~666 nm are replaced by a Chl ESA.

CP26, 632 nm excitation

The steady-state absorption spectrum of CP26 shows a characteristic band at 636 nm. To study the EET pathways from this blue-shifted Chl *b*, we performed pump-probe experiments with excitation at 632 nm (Fig. 3 A). The first EADS displays a bleach/SE with peaks at 636 and 677 nm. The presence of excited Chls *a* is likely due to direct excitation of Chls *a* in the Q_y vibrational band, which is likely Chl *a*-unspecific. Notably, the EADS is flat in the 643–662 nm range, suggesting that other excited Chls *b* are not present in the spectrum. The second spectrum appears in 1.1 ps and shows a decay of the Chls *b* at 636 nm and a rise in the Chl *a* region, with a maximum at 678 nm and a pronounced shoulder at ~670 nm. No excitation transfer between Chls *b* has taken place, since no trace of excited Chls *b* around 650 nm is visible. The second 7.9 ps evolution shows equilibration within the Chl *a* band with the loss of blue Chl *a* around 670 nm. In contrast to the other data sets, a fit with four components (not shown) yielded no significant improvements in the fit.

CP24, 652 nm excitation

The fit shown in Fig. 4 B was accomplished with four components plus an additional one for the rise of the CarT at late delay times (Fig. 5). The first EADS is composed of a bleach/SE at 650 nm and a sharp feature at 670 nm. Similarly to CP26, the Chl *b* bleaching is asymmetrically broadened on the low-energy side. This indicates the presence of different Chl *b* pools in the bleaching. In the second component appearing in 610 fs, the area of the Chl *b* bands has decreased by 86%. Two distinct narrow bands appear with peaks at 670 and 676 nm, mostly as a result of EET from the Chls *b*. Similarly to CP26, the first two DADS (Fig. S2) show a red shift of the decaying Chl *b* bands, implying that a Chl *b* population at relatively high energies has decayed in the first sub-ps phase. In the third spectrum rising in 3.6 ps, the complete decay of the Chl *b* excited states and the band at 670 nm can be observed. The main bleach/SE of the Chl *a* region at 677 nm originates from excited Chls *a* absorbing at low energies. As compared to the last spectrum, the 30 ps EADS appears slightly broadened on the high-energy side. The last spectrum in fact shows a shift of 1.1 nm to higher wavelengths. This is the result of a decay

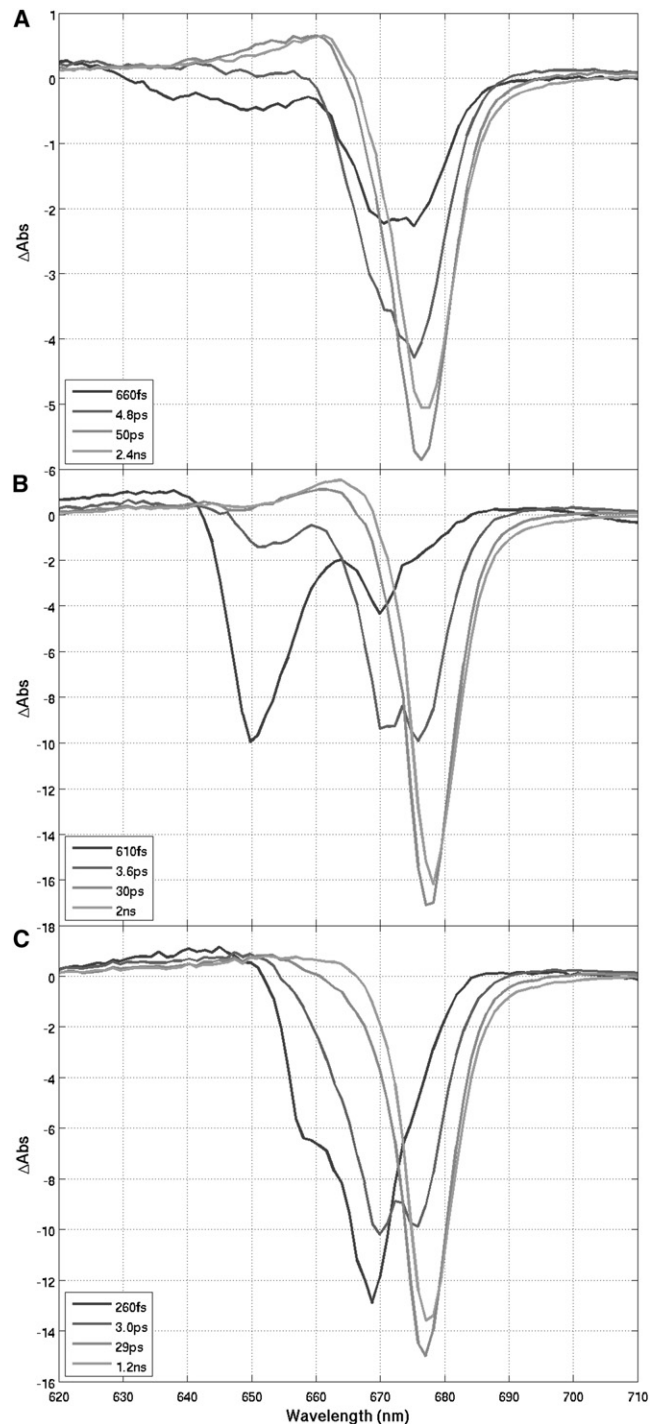


FIGURE 4 Global analysis of CP24 excited at 632 nm (A), 652 (B), and 661 nm (C).

in the high-energy side of the Q_y peak, due to slow recombination within different Chl *a* populations.

CP24, 661 nm excitation

The first EADS of the 661 nm excitation experiment (Fig. 4 C) shows a broad bleach/SE at 669 nm flanked by

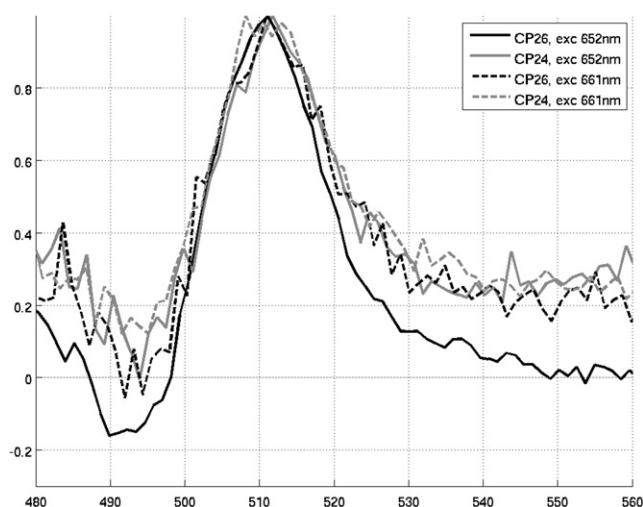


FIGURE 5 EADS with infinite lifetime of the global analyses in Figs. 3, A–C, and 4, A–C, describing CarT formation at late delay times. The spectra were normalized for clarity.

a band at 658 nm, and a small shoulder on the high-energy side at ~675 nm. Chl *b* signal is present below 490 nm only in the first EADS (not shown). Based on quantitative estimations of the Soret and Chl *b* Q_y bleaching areas, we conclude that the whole band at 658 nm originates from excited Chls *b*. The presence of different Chl populations in the spectrum implies that part of the 676 nm band visible in the second EADS has already occurred, either via direct excitation by the pump beam or by ultrafast EET from other Chls at higher energies. Similar to the 652 nm data of Fig. 4 B, in the second EADS the same two peaks at 670 and 676 nm of Fig. 4 B are present. This means that the first dynamics in the 652 and 661 nm data sets are analogous. Remarkably, the 670 nm band has not grown in the first evolution of Fig. 4 C, implying that this band has not received excitations from excited Chl absorbing around 658 nm. Therefore, in the first evolution, the red Chls *b* forming the shoulder at 658 nm show EET uniquely to the band at 676 nm. The two slowest lifetimes provided by the global analyses in Fig. 5, B and C, are similar. They describe the decay of the 670 nm band and the equilibration between the Chl *a* bands peaking at 676/677 nm.

CP24, 632 nm excitation

A global analysis for the pump-probe experiments on CP24 excited at 632 nm is shown in Fig. 4 A. In the first EADS, Chl *b* bleach/SE bands are spread over the whole Chl *b* Q_y region, with discernible bands at 638 and ~650 nm. The two Chl *a* bands seen in the previous data sets are also present at 671 and 675 nm. Part of these excited Chl *a* bands are the result of direct excitation, due to the background absorption of vibronic transitions. In the second spectrum appearing in 660 fs, the Chls *b* absorbing at high energies have completely

decayed, whereas some residual Chls *b* in the 645–660 nm region are still excited and overlap with the Chl *a* ESA. The Chl *a* bleach/SE has increased and the ratio between the two bands has changed, suggesting that EET has favored the 675 nm band. In the third EADS, appearing in 4.8 ps, the main bleach narrows and shifts to 676 nm because of the decay of the 670 nm Chl *a* band. Therefore, one can conclude that the dynamics after the first evolution are similar to those of the 652 nm data set, as evidenced by the build-up of the same bands at ~670 and 675 nm, followed by relaxation in the second picosecond evolution. The final transition shows the relaxation among Chls *a*.

DISCUSSION

Femtosecond TA measurements on the antenna proteins CP26 (Lhcb5) and CP24 (Lhcb6) of PSII provide information about the excitation energy dynamics in these complexes. Although it is not possible to produce a complete model for the EET in these antennas in the absence of an atomic structure of the complexes, one can attempt to explain the observed dynamics in the structural framework by combining the information about Chl assignment provided by mutation analysis (25,26) with the LHCII exciton model (2,3,27,48). This approach allows us to assign most of the dynamics and compare the EETs in individual complexes. The characteristic lifetimes observed are summarized in Tables 2 and 3 along with qualitative assignments.

CP26

Stoichiometric data indicate that CP26 coordinates nine Chls (six Chls *a* and three Chls *b* (15)), and it has been suggested that, as compared to LHCII, Chls 601, 604, 605, 607, and 608 are missing (25). In the TA data, three Chl *b* to Chl *a* EET components were observed in CP26: 210 fs and 1.5 ps from Chls *b* absorbing at 650 nm and 1.1 ps for

TABLE 2 Summary of observed lifetimes and spectral positions, and assignment of components for CP26

Lifetime (ps)	Spectral position (nm)	Assignment
<0.1	660–680	Chl <i>b</i> to Chl <i>a</i> transfer and/or Chl <i>a</i> Q _x state relaxation
0.21	650, 653	Chl <i>b</i> to Chl <i>a</i> transfer
	660–665	Chl <i>b</i> and <i>a</i> to Chl <i>a</i> transfer
0.32	655–670	Chl <i>b</i> (25%) and Chl <i>a</i> (75%) to Chl <i>a</i> transfer
1.1	636	Chl <i>b</i> to Chl <i>a</i> transfer
1.5	653	Chl <i>a</i> to Chl <i>a</i> transfer
1.5–3.5	666–668	Chl <i>a</i> to Chl <i>a</i> transfer
10–15	660–690	Equilibration within Chl <i>a</i> bands
1–2 ns	670–690	Chl <i>a</i> excited states decay
	480–530	CarT formation

TABLE 3 Summary of observed lifetimes and spectral positions, and assignment of components for CP24

Lifetime (ps)	Spectral position (nm)	Assignment
<0.1	670	Chl <i>b</i> to Chl <i>a</i> transfer and/or Chl <i>a</i> Q _x state relaxation
0.26	658	Chl <i>b</i> to Chl <i>a</i> transfer
	670	Chl <i>a</i> to Chl <i>a</i> transfer
0.61	649, 654	Chl <i>b</i> to Chl <i>a</i> -670 and Chl <i>a</i> -675 nm transfer
0.66	636	Chl <i>b</i> to Chl <i>a</i> transfer
3	655–665	Chl <i>a</i> to Chl <i>a</i> transfer
3.0–4.8	670	Chl <i>a</i> to Chl <i>a</i> transfer
4.8	645–655	Chl <i>b</i> to Chl <i>a</i> transfer
30	660–690	Equilibration within Chl <i>a</i> bands
1–2 ns	670–690	Chl <i>a</i> excited states decay
	480–530	CarT formation

a Chl *b* form at 636 nm. One distinctive feature of CP26 compared to LHCII is the reduction of the slow Chl *b* decay lifetime, from 3.3 ps (33) to 1.5 ps. In addition, the corresponding EADS show smaller amplitudes of the intermediate states (660–670 nm). These indications suggest that the overall EET to the low-energy states occurs more rapidly in CP26. According to the energy level diagram in Fig. 8 of van Grondelle and Novoderezhkin (2), the EET from the *b*606-*b*607 pair to the bottleneck states Chl *b*605 and Chl *a*604 describes the slow dynamics in both Chl *b* and *a* bands in LHCII. The proposed lack in CP26 of both bottleneck Chls destroys the EET pathway from the *b*606-*b*607 pair to the remaining Chls. The result is the suppression of the slowest Chl *b* to Chl *a* EET process.

Neglecting the possible ultrafast population of Chls *a*, a single sub-ps component is sufficient for a global fit of the Chl *b* dynamics. The absence of a sub-ps component in CP26, in contrast to LHCII (where two components of 0.13 and 0.6 ps are present), is very likely related to the absence of Chls *b*607 and *b*608 in the former complex (25).

The measurements also show that the Chl *b* absorbing at 636 nm does not transfer energy to other Chl *b* molecules. Mutation analysis suggests that the 636 nm form is associated with Chl 606 (25). The absence of transfer from this Chl *b* to other Chls *b* is in agreement with the absence in CP26 of Chls 607 and 605, which in LHCII are located close to Chl 606. However, in the framework of the LHCII model, the 1.1 ps transfer from this 636 nm species seems much too fast for a Chl that it is expected to be relatively isolated (considering the LHCII structure, the closest Chl should be Chl 609 at 14 Å). On the other hand, we should take into account that the ligand for Chl 606 in LHCII is a Gln, whereas it is a Glu in CP26. This substitution has been shown to strongly influence the hydrogen-bond network that stabilizes the C-helix domain. As a result, this is the main factor responsible for the difference in the pigment binding and organization in this domain between CP29 and LHCII (21,22). In this respect, CP26 is expected

to be very similar to CP29. Indeed, TA measurements on CP29 show that the transfer from the 640 nm form occurs in 600–900 fs to a blue Chl *a*, without the involvement of other Chl *b* forms (37,49), exactly as in CP26. On the basis of these considerations, we thus attribute the 1.1 ps component to EET from Chl 606.

As regards the forms in the intermediate-states region, both fast and slow dynamics are visible in the data. In the 661 nm data, the fast 320 fs transfer originates in part from a fraction of red Chls *b* absorbing roughly below 660 nm, but in great measure (~75%) from blue Chls *a* (at 665 nm). According to the excitonic model of LHCII, slow dynamics could be explained by the presence of a Chl *a* in the 604 site. However, the assignment of the *a*604 is problematic because mutation analysis cannot directly target this site. As a consequence, the absence of Chl 604 was suggested only on the basis of stoichiometry considerations (26). On the other hand, it was also shown (50) that the absence of Neo influences the absorption of an unidentified Chl *a*, which in principle could be Chl *a*604, since it is the closest Chl *a* to Neo (3.3 Å). Moreover, we observe that these slow forms are absent in the third transitions of CP24. This suggests that Chl *a*613 and/or *a*614, which CP24 lacks, may be involved.

Mutation analysis (25) showed that the absorption form at 665 nm is associated with Chl 614, whereas the Chl *a* in the *a*613 site was suggested to absorb at 678 nm. In the exciton model (2), the relaxation time from the lumenal-side Chl *a*613 (and Chl *a*614) to the red states was estimated in the ps regime (V. I. Novoderezhkin, A. Marin, and R. van Grondelle, unpublished data), making Chl *a*613 a possible candidate for the slow dynamics around 665 nm.

CP24

Stoichiometric and mutagenesis information obtained from the CP24 complex indicates that two Chl *b* clusters are conserved as compared to LHCII, *b*606-*b*607, and *b*608-*b*609, whereas the fifth Chl *b* is suggested to be associated with site 604 (based on indirect observations). Two Chl-binding sites, Chl *a*613 and *a*614, are absent in CP24, in contrast to LHCII (in addition to the labile *b*605 and *b*601 sites, which are absent in all reconstituted complexes) (26). In all CP24 data sets, evidence was found for three Chl *a* bands located at ~670, 675, and 678–680 nm. Similarly, we can resolve at least three Chl *b* bands at 638, 650, and 653–654 nm, to be assigned to the 5 Chls *b* present in the complex.

Notably, most of the Chl *b* to Chl *a* transfer (86%) in CP24 occurs in the sub-ps range, indicating efficient overall EET from Chl *b* to Chl *a*, and suggesting a functional disruption of the bottleneck Chls in the 604 and 605 sites.

As in CP26, one high-energy Chl form must account for the shoulder at 637.5 nm in the OD spectrum. The main

difference between the 632 nm data sets of CP26 and CP24 is that in CP24, Chls *b* absorbing at 650 nm get involved in the fast excitation transfer dynamics originating from the 637 form. This can easily be explained by considering that CP24 is very rich in Chls *b*, especially in the neighborhood of Chl 606, whereas this is not the case in CP26. The attribution of the absorption at 637.5 nm to Chl *b*606 in CP24 can also explain the relaxation pathways to the Chl 604 and/or Chl *b*607 site.

The 652 nm excitation data set shows the transfer from two Chl *b* populations to two Chl *a* bands at 670 and 674.5 (cf. DADS in Fig. S2). The first evolution occurs only in 610 fs, indicating a reduced fast Chl *b* to Chl *a* transfer in CP24. It is interesting to note that in both the 652 and 661 nm excitation data sets, the spectra at time zero show little Chl *a* bleaching above 670 nm, but a pronounced narrow band at 670 nm. This suggests that most of the Chls *b* do not seem to strongly interact with the low-energy states Chls *a*. This is in agreement with the proposed assignment that all Chls *b* are clustered in the C-helix domain and thus are far from Chl *a*611 and *a*612, which accommodate the lowest-energy state (26).

The most probable assignment of the 670 nm band is to Chl *a*602 or *a*603. In favor of this assignment, the 2.5–3 ps migration time from this Chl *a* cluster to others, as estimated by the LHCII model, is consistent with our observations when the faster transitions to the *a*613–*a*614 Chls *a* are neglected (as is the case with CP24, where these two Chls are not present). Alternatively, evidence was found that Chl *a*610 does not contribute to the low-energy state of the complex (26) and instead absorbs at 670 nm. However, in this case, a transfer time of 3 ps seems too slow for a correct description of the dynamics between Chl *a*610 and the Chl *a*611/*a*612 pair; these Chls are clustered in the stromal layer of the complex, as also indicated in CP24 by mutation analysis (26). This assignment leads to the conclusion that a large part of the 650 nm excitation passes through Chl *a*602/*a*603 before reaching the lowest-energy state.

CONCLUSIONS

In this work, we studied the excited-state dynamics of the minor antenna complexes CP24 and CP26 in detail by TA upon excitation at different wavelengths in the Q_y region. The dynamics in CP26 are rather similar to those of LHCII, with two exceptions: the reduction of the contribution of the bottleneck states, and the presence of only one sub-ps Chl *b* to Chl *a* transfer component. Both observations could be explained by the absence in CP26 of specific Chls. However, one can conclude that in terms of its EET dynamics, CP26 strongly resembles LHCII. This suggests a very similar structure and pigment organization, in agreement with previous data (43,51). This is also in line with the fact that, in the absence of LHCII, CP26 is able to form trimers

and to substitute LHCII in the PSII supercomplex (52). The high similarity between the two complexes suggests that this substitution would have a minor influence on the light-harvesting properties of the PSII supercomplexes and thus on the functioning of the system.

At variance with CP26, CP24 shows clearly different dynamics as compared to LHCII. First, this complex is strongly enriched in 670 nm forms with a narrow spectrum. Furthermore, most of the transfer from Chl *b* to Chl *a* occurs in 610 fs and is directed toward Chl *a*602 and/or Chl *a*603, thereby mediating a large part of the transfer to the lowest-energy state. These two Chls in CP24 seem to play a special role: Chl *a*603 has been suggested to be a quenching site (53), and the occupancy of the Car L2 site, located close to Chl 603, has been shown to modulate quenching (26). Moreover, mutation analysis shows that, in contrast to the other antenna complexes, the mutants affecting these two binding sites are not stable (26), suggesting an important functional role for these Chls. A large part of the excitation is intercepted by these Chls before they reach the lowest-energy state, from which energy is transferred to the next complex (11). Thus, these Chls may have a functional role in regulating transfer and/or quenching when, under stress conditions, CP24 dissociates from the PSII supercomplex (54).

SUPPORTING MATERIAL

Two figures are available at [http://www.biophysj.org/biophysj/supplemental/S0006-3495\(10\)01322-6](http://www.biophysj.org/biophysj/supplemental/S0006-3495(10)01322-6).

We thank Stefano Caffarri for the generous gift of the reconstituted CP26 sample, Jos Thieme for technical assistance, Vladimir Novoderezhkin for useful discussions and material, Ivo van Stokkum for his guidance during the data analysis, and John Kennis for organizing the access to the multi-pulse setup. A.M. thanks Fred Etoc for fruitful discussions.

This work was supported by the Netherlands Organization for Scientific Research-Chemical Sciences through a TOP grant to R.v.G., Earth and Life Science, and a Vidi grant to R.C.

REFERENCES

1. van Amerongen, H., and R. van Grondelle. 2001. Understanding the energy transfer function of LHCII, the major light-harvesting complex of green plants. *J. Phys. Chem. B.* 105:604–617.
2. van Grondelle, R., and V. I. Novoderezhkin. 2006. Energy transfer in photosynthesis: experimental insights and quantitative models. *Phys. Chem. Chem. Phys.* 8:793–807.
3. Novoderezhkin, V. I., and R. van Grondelle. 2010. Physical origins and models of energy transfer in photosynthetic light-harvesting. *Phys. Chem. Chem. Phys.* 12:7352–7365.
4. Horton, P., A. V. Ruban, and R. G. Walters. 1996. Regulation of light harvesting in green plants. *Annu. Rev. Plant Physiol. Plant Mol. Biol.* 47:655–684.
5. Demmig-Adams, B., and W. I. Adams. 1992. Photoprotection and other responses of plants to high light stress. *Annu. Rev. Plant Physiol.* 43:599–626.
6. Niyogi, K. K. 1999. Photoprotection revisited: genetic and molecular approaches. *Annu. Rev. Plant Physiol. Plant Mol. Biol.* 50:333–359.

7. Holt, N. E., D. Zigmantas, ..., G. R. Fleming. 2005. Carotenoid cation formation and the regulation of photosynthetic light harvesting. *Science*. 307:433–436.
8. Ruban, A. V., R. Berera, ..., R. van Grondelle. 2007. Identification of a mechanism of photoprotective energy dissipation in higher plants. *Nature*. 450:575–578.
9. Jansson, S. 1999. A guide to the Lhc genes and their relatives in *Arabidopsis*. *Trends Plant Sci.* 4:236–240.
10. Boekema, E. J., H. van Roon, ..., J. P. Dekker. 1999. Multiple types of association of photosystem II and its light-harvesting antenna in partially solubilized photosystem II membranes. *Biochemistry*. 38:2233–2239.
11. Caffarri, S., R. Kouril, ..., R. Croce. 2009. Functional architecture of higher plant photosystem II supercomplexes. *EMBO J.* 28:3052–3063.
12. Liu, Z., H. Yan, ..., W. Chang. 2004. Crystal structure of spinach major light-harvesting complex at 2.72 Å resolution. *Nature*. 428:287–292.
13. Standfuss, J., A. C. Terwisscha van Scheltinga, ..., W. Kühlbrandt. 2005. Mechanisms of photoprotection and nonphotochemical quenching in pea light-harvesting complex at 2.5 Å resolution. *EMBO J.* 24:919–928.
14. Jansson, S. 1994. The light-harvesting chlorophyll a/b-binding proteins. *Biochim. Biophys. Acta*. 1184:1–19.
15. Dainese, P., and R. Bassi. 1991. Subunit stoichiometry of the chloroplast photosystem II antenna system and aggregation state of the component chlorophyll a/b binding proteins. *J. Biol. Chem.* 266:8136–8142.
16. Sandonà, D., R. Croce, ..., R. Bassi. 1998. Higher plants light harvesting proteins. Structure and function as revealed by mutation analysis of either protein or chromophore moieties. *Biochim. Biophys. Acta*. 1365:207–214.
17. Plumley, F. G., and G. W. Schmidt. 1987. Reconstitution of chlorophyll a/b light-harvesting complexes: Xanthophyll-dependent assembly and energy transfer. *Proc. Natl. Acad. Sci. USA*. 84:146–150.
18. Paulsen, H., U. Rumler, and W. Rudiger. 1990. Reconstitution of chlorophyll pigment-containing complexes from light-harvesting chlorophyll a/b-binding protein overexpressed in *Escherichia coli*. *Planta*. 181:204–211.
19. Paulsen, H., B. Finkenzeller, and N. Kühlein. 1993. Pigments induce folding of light-harvesting chlorophyll a/b-binding protein. *Eur. J. Biochem.* 215:809–816.
20. Giuffra, E., D. Cugini, ..., R. Bassi. 1996. Reconstitution and pigment-binding properties of recombinant CP29. *Eur. J. Biochem.* 238:112–120.
21. Bassi, R., R. Croce, ..., D. Sandonà. 1999. Mutational analysis of a higher plant antenna protein provides identification of chromophores bound into multiple sites. *Proc. Natl. Acad. Sci. USA*. 96:10056–10061.
22. Remelli, R., C. Varotto, ..., R. Bassi. 1999. Chlorophyll binding to monomeric light-harvesting complex. A mutation analysis of chromophore-binding residues. *J. Biol. Chem.* 274:33510–33521.
23. Hobe, S., I. Trostmann, ..., H. Paulsen. 2006. Assembly of the major light-harvesting chlorophyll-a/b complex: thermodynamics and kinetics of neoxanthin binding. *J. Biol. Chem.* 281:25156–25166.
24. Simonetto, R., M. Crimi, ..., R. Bassi. 1999. Orientation of chlorophyll transition moments in the higher-plant light-harvesting complex CP29. *Biochemistry*. 38:12974–12983.
25. Ballottari, M., M. Mozzo, ..., R. Bassi. 2009. Occupancy and functional architecture of the pigment binding sites of photosystem II antenna complex Lhcb5. *J. Biol. Chem.* 284:8103–8113.
26. Passarini, F., E. Wientjes, ..., R. Croce. 2009. Molecular basis of light harvesting and photoprotection in CP24: unique features of the most recent antenna complex. *J. Biol. Chem.* 284:29536–29546.
27. Novoderezhkin, V. I., M. A. Palacios, ..., R. van Grondelle. 2005. Excitation dynamics in the LHClI complex of higher plants: modeling based on the 2.72 Ångström crystal structure. *J. Phys. Chem. B*. 109:10493–10504.
28. Cinque, G., R. Croce, ..., R. Bassi. 2000. Energy transfer among CP29 chlorophylls: calculated Förster rates and experimental transient absorption at room temperature. *Biophys. J.* 79:1706–1717.
29. Visser, H. M., F. J. Kleima, ..., H. van Amerongen. 1996. Probing the many energy-transfer processes in the photosynthetic light-harvesting complex II at 77 K using energy-selective sub-picosecond transient absorption spectroscopy. *Chem. Phys.* 210:297–312.
30. Visser, H., F. Kleima, ..., H. van Amerongen. 1997. Probing the many energy-transfer processes in the photosynthetic light-harvesting complex II at 77 K using energy-selective sub-picosecond transient absorption spectroscopy. *Chem. Phys.* 215:299.
31. Kleima, F. J., C. C. Gradinaru, ..., H. van Amerongen. 1997. Energy transfer in LHClI monomers at 77K studied by sub-picosecond transient absorption spectroscopy. *Biochemistry*. 36:15262–15268.
32. Gradinaru, C. C., S. Ozdemir, ..., H. van Amerongen. 1998. The flow of excitation energy in LHClI monomers: implications for the structural model of the major plant antenna. *Biophys. J.* 75:3064–3077.
33. Palacios, M. A., J. Standfuss, ..., R. van Grondelle. 2006. A comparison of the three isoforms of the light-harvesting complex II using transient absorption and time-resolved fluorescence measurements. *Photosynth. Res.* 88:269–285.
34. Connelly, J. P., M. G. Müller, ..., A. R. Holzwarth. 1997. Femtosecond transient absorption study of carotenoid to chlorophyll energy transfer in the light-harvesting complex II of photosystem II. *Biochemistry*. 36:281–287.
35. Cinque, G., R. Croce, and R. Bassi. 2000. Absorption spectra of chlorophyll a and b in Lhcb protein environment. *Photosynth. Res.* 64:233–242.
36. Croce, R., M. G. Müller, ..., A. R. Holzwarth. 2003. Energy transfer pathways in the minor antenna complex CP29 of photosystem II: a femtosecond study of carotenoid to chlorophyll transfer on mutant and WT complexes. *Biophys. J.* 84:2517–2532.
37. Croce, R., M. G. Müller, ..., A. R. Holzwarth. 2003. Chlorophyll b to chlorophyll a energy transfer kinetics in the CP29 antenna complex: a comparative femtosecond absorption study between native and reconstituted proteins. *Biophys. J.* 84:2508–2516.
38. Gradinaru, C. C., A. A. Pascal, ..., H. van Amerongen. 1998. Ultrafast evolution of the excited states in the chlorophyll a/b complex CP29 from green plants studied by energy-selective pump-probe spectroscopy. *Biochemistry*. 37:1143–1149.
39. Gradinaru, C., I. van Stokkum, ..., H. van Amerongen. 2000. Identifying the pathways of energy transfer between carotenoids and chlorophylls in LHClI and CP29. A multicolor pump-probe study. *J. Phys. Chem.* 104:9330–9342.
40. Savikhin, S., H. van Amerongen, ..., W. S. Struve. 1994. Low-temperature energy transfer in LHC-II trimers of the Chl a/b light-harvesting antenna of photosystem II. *Biophys. J.* 66:1597–1603.
41. Croce, R., S. Weiss, and R. Bassi. 1999. Carotenoid-binding sites of the major light-harvesting complex II of higher plants. *J. Biol. Chem.* 274:29613–29623.
42. Gilmore, A. M., and H. Y. Yamamoto. 1991. Zeaxanthin formation and energy-dependent fluorescence quenching in pea chloroplasts under artificially mediated linear and cyclic electron transport. *Plant Physiol.* 96:635–643.
43. Croce, R., G. Canino, ..., R. Bassi. 2002. Chromophore organization in the higher-plant photosystem II antenna protein CP26. *Biochemistry*. 41:7334–7343.
44. van Stokkum, I. H. M., D. S. Larsen, and R. van Grondelle. 2004. Global and target analysis of time-resolved spectra. *Biochim. Biophys. Acta*. 1657:82–104.
45. Schödel, R., K. D. Irrgang, ..., G. Renger. 1999. Quenching of chlorophyll fluorescence by triplets in solubilized light-harvesting complex II (LHClI). *Biophys. J.* 76:2238–2248.
46. Mozzo, M., L. Dall'Osto, ..., R. Croce. 2008. Photoprotection in the antenna complexes of photosystem II: role of individual xanthophylls in chlorophyll triplet quenching. *J. Biol. Chem.* 283:6184–6192.

47. Mozzo, M., F. Passarini, ..., R. Croce. 2008. Photoprotection in higher plants: the putative quenching site is conserved in all outer light-harvesting complexes of Photosystem II. *Biochim. Biophys. Acta.* 1777:1263–1267.
48. Novoderezhkin, V., J. Salverda, ..., R. van Grondelle. 2003. Exciton modeling of energy-transfer dynamics in the LHClI complex of higher plants: a Redfield theory approach. *J. Phys. Chem. B.* 107:1893–1912.
49. Pieper, J., K. D. Irrgang, ..., G. J. Small. 2000. Assignment of the lowest Qy-state and spectral dynamics of the CP29 chlorophyll a/b antenna complex of green plants: a hole-burning study. *Photochem. Photobiol.* 71:574–581.
50. Caffarri, S., F. Passarini, ..., R. Croce. 2007. A specific binding site for neoxanthin in the monomeric antenna proteins CP26 and CP29 of Photosystem II. *FEBS Lett.* 581:4704–4710.
51. Frank, H. A., S. K. Das, ..., R. Bassi. 2001. Photochemical behavior of xanthophylls in the recombinant photosystem II antenna complex, CP26. *Biochemistry.* 40:1220–1225.
52. Ruban, A. V., M. Wentworth, ..., P. Horton. 2003. Plants lacking the main light-harvesting complex retain photosystem II macro-organization. *Nature.* 421:648–652.
53. Ahn, T. K., T. J. Avenson, ..., G. R. Fleming. 2008. Architecture of a charge-transfer state regulating light harvesting in a plant antenna protein. *Science.* 320:794–797.
54. Betterle, N., M. Ballottari, ..., R. Bassi. 2009. Light-induced dissociation of an antenna hetero-oligomer is needed for non-photochemical quenching induction. *J. Biol. Chem.* 284:15255–15266.